

# Spin injection and electric field effect in degenerate semiconductors

Irene D'Amico

*Istituto Nazionale per la Fisica della Materia (INFM);  
Institute for Scientific Interchange, via Settimio Severo 65, I-10133 Torino, Italy*

Giovanni Vignale

*Department of Physics, University of Missouri, Columbia, Missouri 65211  
(Dated: May 22, 2019)*

We analyze spin-transport in semiconductors in the regime characterized by  $T \lesssim T_F$  (intermediate to degenerate), where  $T_F$  is the Fermi temperature. Such regime is of great importance since it includes the lightly doped semiconductor structures used in most experiments; we demonstrate that, at the same time, it corresponds to the regime in which carrier-carrier interactions can assume a relevant role.

We derive a general formalism which can be applied to ferromagnet/non-magnetic semiconductor junctions independently from the semiconductor regime.

We analyze in details the combined effect of carrier density variation, applied electric field and Coulomb interactions on spin injection and concentrate on a *degenerate* regime peculiar to semiconductors, which strongly differs, as spin-transport is concerned, from the well known degenerate regime of metals.

PACS numbers: 72.25.-b, 72.10.-d, 72.25.Dc

## I. INTRODUCTION

Despite many efforts and substantial progresses, major difficulties persist when considering practical implementation of spintronics devices. It has been recently pointed out a fundamental problem inherent the electrical injection of spin currents into semiconductors<sup>1</sup>, the so-called conductivity mismatch: the large conductivity difference between metals and semiconductors induces a spin accumulation at the interface which in turn drastically reduces spin injection into the semiconductor. Another critical issue is to preserve and enhance a spin current inside the medium: due to the finite spin-flip length, the spin-current tends to decay after injection. It has been shown that this may be improved by applying a strong electric field<sup>2</sup>, which may enhance the penetration of the spin-current. The analysis was done in the non-interacting approximation and considered non-magnetic semiconductors in the non-degenerate regime when studying heterostructures.

In this article we will derive a general formalism (which includes Coulomb interactions) for studying heterostructures independently on the non-magnetic semiconductor (NMS) carrier density regime. We will then focus in our discussion on NMS in the *intermediate and degenerate* regime, i.e. characterized by  $T \lesssim T_F$ , where  $T_F = \epsilon_F/k_B$  is the Fermi temperature. Such regime is of utmost importance since it includes most of the semiconductor structures used in spintronics related experiments, such as n-doped GaAs<sup>3</sup> or Zn<sub>0.97</sub>Be<sub>0.03</sub>Se<sup>4</sup> ones. This is illustrated in Fig. 1, where we plot the ratio  $T/T_F$  in respect to the carrier density  $n$  for n-doped GaAs (upper panel) and (Zn,Be)Se (lower panel). Three different values of the temperature are considered (as labelled). The regions corresponding to degenerate and non-degenerate

systems are specified as well. As can be seen, up to room temperatures, for densities as low as  $n \sim 5 \cdot 10^{16} \text{ cm}^{-3}$  in GaAs or  $n \sim 10^{18} \text{ cm}^{-3}$  in (Zn,Be)Se the system is at most in the intermediate regime; a system at  $T = 1.6 \text{ K}$ , a temperature often used in experiments, remains in the *degenerate* regime  $T/T_F \ll 1$  for the whole relevant density range.

For its importance, in this article we will mainly discuss n-doped GaAs at  $T = 1.6 \text{ K}$ ; our results are based on the interplay among different energy scales, so they can be readily extended to other semiconductor materials.

We will analyze the interplay between electric field, different carrier densities and Coulomb interactions on spin transport and spin injection. We will show that, due to the strong dependence of the spin diffusion constant on carrier density (see inset of Fig. 1), it is possible to greatly enhance the local spin current density by carefully choosing the system parameters.

The paper is organized as follow: in Sec. II we will derive the drift diffusion equation for spin-transport including Coulomb interactions and we will discuss the effects of interactions and carrier density on the diffusion lengths; in Sec. III we will consider the spin current and the implications of varying the carrier density on such quantity; in Sec. IV we will introduce a general formalism to express the electrochemical potential and we will consider ferromagnet/NMS heterostructure; in Sec. V we will study a ferromagnet/NMS/ferromagnet (FM) system and finally Sec. VI will be devoted to a short summary and conclusions.

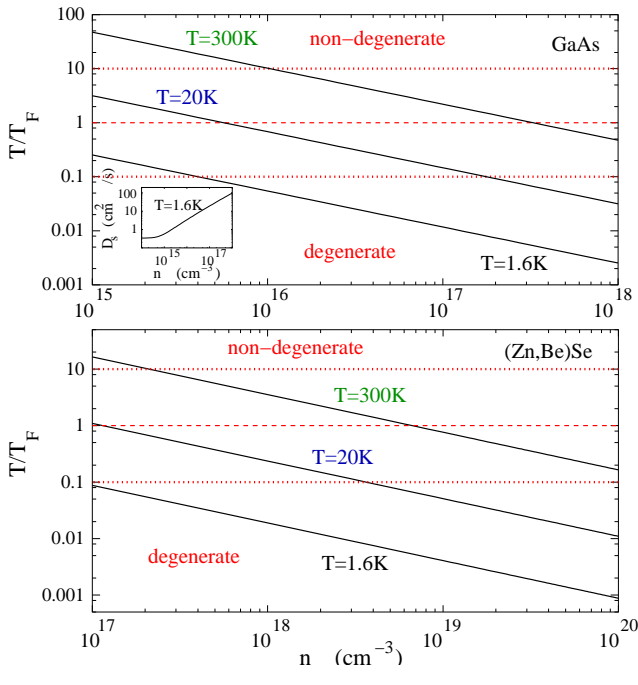


FIG. 1:  $T/T_F$  vs carrier density  $n$  for GaAs (upper panel,  $m = 0.067m_0$ ,  $\epsilon = 12$ ) and (Zn, Be)Se (lower panel,  $m = 0.5m_0$ ,  $\epsilon = 12$ ) parameters, at  $T = 1.6K$ ,  $20K$ ,  $300K$ , as labelled. Degenerate and non-degenerate regions are indicated as well. Inset:  $D_s$  vs carrier density for  $T = 1.6K$  and GaAs parameters.

## II. INTERACTING DRIFT-DIFFUSION EQUATION

First of all we will derive a drift-diffusion equation for steady state spin-transport which *includes Coulomb interactions* between carriers of different spin populations. We proceed as in Ref. 5, to which we refer the reader for the details.

We start from the drift diffusion equation for the interacting spin- $\alpha$  charge current

$$\vec{j}_\alpha(\vec{r}) = \sum_\beta \left( \sigma_{\alpha\beta} \vec{E} + e D_{\alpha\beta} \vec{\nabla} n_\beta \right), \quad (1)$$

where  $\vec{E}$  is the applied electric field,  $\sigma_{\alpha\beta}$  is the homogeneous conductivity matrix of the electron gas,  $D_{\alpha\beta}$  is the diffusion matrix. Throughout the paper Greek indices will correspond to the spin-variables  $\uparrow, \downarrow$ . We substitute Eq. (1) in the generalized continuity equation for the spin-density components

$$\frac{\partial \Delta n_\alpha(\vec{r}, t)}{\partial t} = -\frac{\Delta n_\alpha(\vec{r}, t)}{\tau_{sf,\alpha}} + \frac{\Delta n_{\bar{\alpha}}(\vec{r}, t)}{\tau_{sf,\bar{\alpha}}} + \frac{\vec{\nabla} \cdot \vec{j}_\alpha(\vec{r})}{e}, \quad (2)$$

where  $\Delta n_\alpha(\vec{r}, t) \equiv n_\alpha(\vec{r}, t) - n_\alpha^{(0)}$ ,  $n_\alpha(\vec{r}, t)$  is the  $\alpha$  density component,  $n_\alpha^{(0)}$  its equilibrium value and  $\tau_{sf,\alpha}$  is the  $\alpha$

spin-flip relaxation time. Carefully applying<sup>5</sup> the local charge neutrality constraint

$$\Delta n_\uparrow(r) = -\Delta n_\downarrow(r) \quad (3)$$

and considering the regime linear in  $\nabla n_\alpha$ , the general interacting drift-diffusion equation can be obtained<sup>5</sup>.

Finally, imposing the steady state condition  $\partial(\Delta n_\uparrow - \Delta n_\downarrow)/\partial t = 0$  we obtain the steady-state *interacting* drift-diffusion equation

$$-\frac{(\Delta n_\uparrow - \Delta n_\downarrow)}{\tau_s} + D_s \nabla^2 (\Delta n_\uparrow - \Delta n_\downarrow) + \mu_s \vec{E} \cdot \vec{\nabla} (\Delta n_\uparrow - \Delta n_\downarrow) = 0, \quad (4)$$

where  $\tau_s = (1/\tau_{sf,\uparrow} + 1/\tau_{sf,\downarrow})^{-1}$  is the spin relaxation time, and the effective interacting mobility and diffusion constants are given, for a non-magnetic system<sup>6</sup> by

$$\mu_s = e\tau_D/m^* \quad (5)$$

and

$$D_s = \frac{\mu_s}{e} S n \frac{1}{1 - \rho_{\uparrow\downarrow}/\rho_D}. \quad (6)$$

Here  $\rho_D = m^*/ne^2\tau_D$  is the ordinary Drude resistivity,  $S$  the static longitudinal spin-stiffness,  $n = n_\uparrow + n_\downarrow$  the carrier density and  $\rho_{\uparrow\downarrow}$  the spin-transresistivity, which measures the momentum rate exchanged between spin up and spin down carriers<sup>5,7,8</sup>. Eq. (4) is valid independently of the value of  $T/T_F$ ; it is tempting, since it leads to simpler analytical formulas, to approximate  $D_s$  by its non-degenerate, classical expression. Unfortunately as it was experimentally shown<sup>3</sup> and theoretically confirmed<sup>9</sup>, the spin diffusion constant varies over *orders of magnitude* going from the non-degenerate to the intermediate and degenerate regime (see inset of Fig. 1, in which  $D_s$  in respect to  $n$  is shown for GaAs parameters); as we will show in details, this implies, that, approximating spin transport behavior by non-degenerate expressions in the wrong regime can lead to quite large errors.

Coulomb interactions enter Eq. (4) through the diffusion and mobility constants; in the non-magnetic limit (Eqs. (5) and (6)), through the diffusion constant only. We want to point out that the experimentally important regime  $T \lesssim T_F$  (see Fig. 1), is the same in which Coulomb interactions between carriers of opposite spin become relevant. They enter  $D_s$  by affecting the spin-stiffness  $S$  and generating the spin transresistivity  $\rho_{\uparrow\downarrow}$ <sup>5,7,8</sup>: for  $T \sim T_F$  the spin transresistivity has its maximum and can become of the same order of the Drude resistivity<sup>5</sup>, while for  $T \lesssim T_F$  the spin-stiffness displays the maximum deviation from its non-interacting approximation<sup>5</sup>. These two combined effects *reduce* the non-interacting approximation to  $D_s$  even by 50%, depending on carrier density and temperature<sup>5</sup>. According to their  $D_s$  dependence, Coulomb interaction effects can get amplified in the various quantities of interest, as we will explicitly show for the downstream spin diffusion length.

If the sample is homogeneous and  $\vec{E} \parallel \hat{x}$  the solution to Eq. (4) is given by

$$\Delta n_\uparrow - \Delta n_\downarrow = Ae^{x/L_u} + Be^{-x/L_d} \quad (7)$$

with A, B determined by the boundary conditions and

$$L_{u,d}^{-1} = \pm \frac{\mu_s |E|}{2D_s} + \sqrt{\left(\frac{\mu_s |E|}{2D_s}\right)^2 + \frac{1}{D_s \tau_s}}. \quad (8)$$

$L_{u,d}$  are the *interacting* upstream and downstream “diffusion” lengths<sup>10</sup> (their non-interacting approximation was derived in Ref. 2). Such quantities correspond to the average decay lengths of an injected spin-unbalance in the upstream ( $L_u$ ) and downstream ( $L_d$ ) directions. Again we notice that, in non-magnetic materials, Coulomb interactions enter  $L_{u,d}$  through  $D_s$ .

Few comments are now in order: due to the presence of the external electric field, the system is characterized by *three different energy scales* whose relative magnitude determines the system behavior. Such energies are the Fermi energy  $\varepsilon_F$ , the thermal energy  $k_B T$  and the energy related to the electric field  $e|E|L_s$ , where  $L_s = \sqrt{D_s \tau_s}$  is the diffusion length. Since we have already discussed how in most experimental situations  $k_B T \ll \varepsilon_F$  (see Fig. 1), we will now concentrate on the ratio  $e|E|L_s/\varepsilon_F$ .

In Fig. 2 we plot this ratio as a function of density and for fields up to 1000 V/cm, for both GaAs and (Zn,Be)Se. In both cases we have chosen  $L_s = 2\mu\text{m}$ . We will consider this same value in all the calculations presented<sup>11</sup>. The high and low field regions are explicitly indicated. We notice that, even at very low densities, it is necessary to increase the field well above 100 V/cm in order to enter the high field regime  $e|E|L_s \gg \varepsilon_F$ .

The comparison of the energy scales, as done in Fig. 1 and Fig. 2, is a very efficient way to understand in which regime the considered system is and deduce how and if the electric field is going to affect the diffusion lengths and the spin-transport related quantities. In order to illustrate this point, we are going to analyze the behavior of the penetration lengths  $L_d$  and  $L_u$  as electric field and carrier density change.

The upper panel of Fig. 3 shows the behavior of  $L_d$ , in respect to density for GaAs at  $T=1.6\text{K}$  and  $E = 25\text{V/cm}$ . The solid line represents the fully interacting calculation, the dashed one the non-interacting approximation and the dashed double dot line the non-degenerate limit obtained by setting  $D_s = \mu_s k_B T/e$  in Eq. (8). The inset in Fig. 3 shows the ratio  $e|E|L_s/\varepsilon_F$  for  $E = 25\text{V/cm}$ .

We want to point out the crossovers between the different regimes undergone by the system when the carrier density is increased. At this temperature even at very low densities the system is degenerate ( $\varepsilon_F >> k_B T$ ), so the interesting interplay is between the Fermi energy and the electric field related energy: *at difference with metals*, in semiconductors the Fermi energy can be low enough such that, even for moderate electric fields, we can fulfill the condition  $e|E|L_s >> \varepsilon_F$ . This is what we

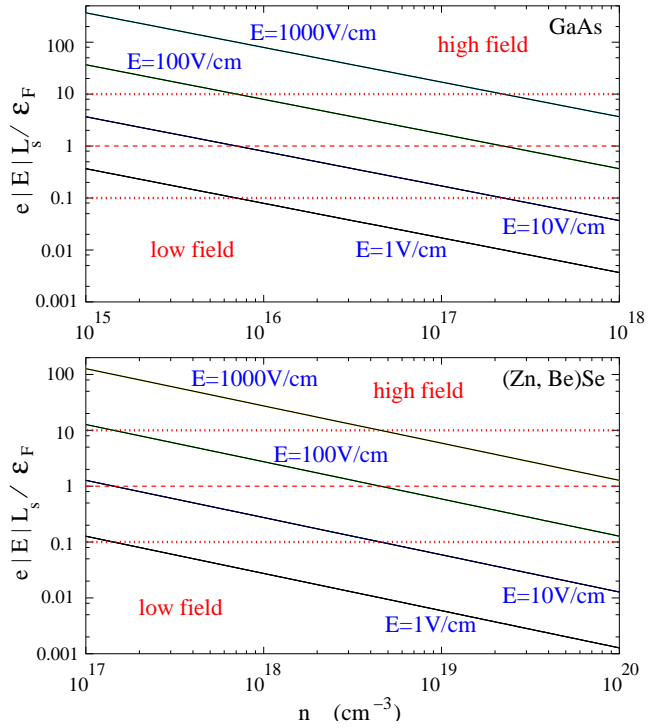


FIG. 2:  $e|E|L_s/\varepsilon_F$  vs carrier density  $n$  for GaAs (upper panel,  $m = 0.067m_0$ ,  $\epsilon = 12$ ) and (Zn, Be)Se (lower panel,  $m = 0.5m_0$ ,  $\epsilon = 12$ ) parameters, for  $E = 1, 10, 100, 1000 \text{ V/cm}$  as labelled. High and low field regions are indicated as well.

define as “semiconductor degenerate regime” to distinguish it from the well-known “metallic” degenerate regime in which  $\varepsilon_F >> e|E|L_s$  for any reasonable field. The existence of such regime implies that, *even for a degenerate system*, the drift term in Eq. (4) cannot be neglected, i.e. it is not possible to describe spin-transport using a diffusion equation for the electrochemical potentials, as usually done for metals<sup>12</sup>. Even in *degenerate* semiconductor systems in fact, the drift term severely modifies the penetration lengths  $L_{u,d}$ , varying their values over order of magnitudes (as clearly shown for  $L_d$  in Fig. 3). As a rule of thumb, we see that in this regime the order of magnitude of such variation is set by the ratio  $e|E|L_s/\varepsilon_F$ . The “semiconductor degenerate” regime extends to higher densities when the applied field is increased. Notice that in such regime the actual value of  $L_d$  strongly differs from its non-degenerate limit.

By increasing the carrier density, the system will eventually enter the “metallic” regime (as indicated in the figure), in which the drift term can be neglected and  $L_{u,d}$  recover their unperturbed value  $L_s$ .

The lower panel of Fig. 3 underlines the importance of Coulomb interactions for such semiconductor system: we plot in fact the correction to the non-interacting value  $(L_d^i - L_d^{ni})/L_d^{ni}$ , where  $i, ni$  stay for interacting and non-interacting respectively, in respect to carrier

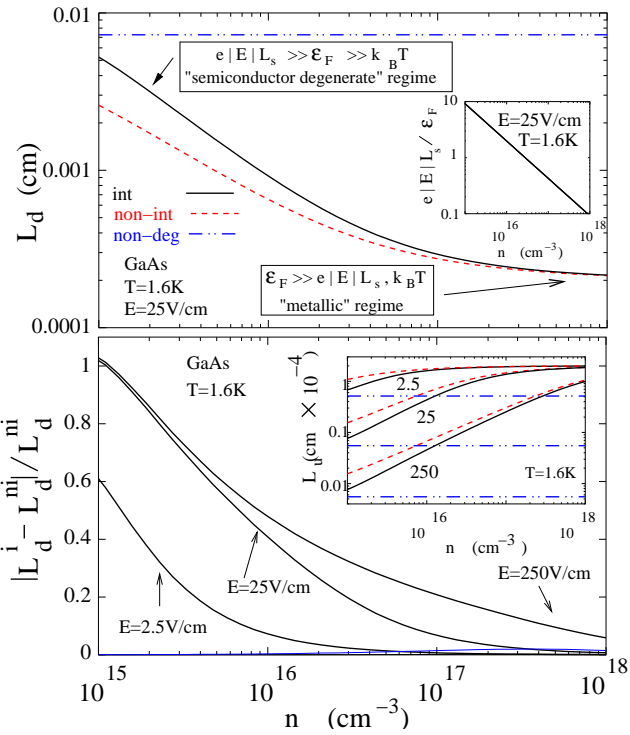


FIG. 3: Upper panel: downstream diffusion length  $L_d$  vs carrier density for GaAs parameters,  $T=1.6K$  and  $E=25V/cm$ . Solid line refers to the full interacting calculation, dashed line to the non-interacting approximation and dashed-double dotted line to the non-degenerate limit. Inset:  $e|E|L_s/\epsilon_F$  vs carrier density for the same parameters as main panel. Lower panel: correction to the non-interacting approximation  $|L_d^i - L_d^{ni}|/L_d^{ni}$  vs carrier density for GaAs parameters,  $T=1.6K$  and three different electric fields (as labelled). Inset: Upstream diffusion length  $L_u$  vs density  $n$  for GaAs parameters at  $T = 1.6K$  and three different fields (as labelled in  $V/cm$  units). Line type as in the main upper panel.

density and for different fields. As one can see, the correction can be of the order of 100%, definitely non-negligible when quantitative calculations are required. Such correction becomes the largest in the high field regime<sup>13</sup>  $e|E|L_s \gg \epsilon_F \gg K_B T$ , when the penetration lengths approach their high field limits  $L_d \approx L_s^2 E \mu_s / D_s$ ,  $L_u \approx D_s / (E \mu_s)$ , which strongly depend over the diffusion constant. At low densities such limiting behavior is reached already for  $E = 25V/cm$ , while the curve corresponding to  $E = 2.5V/cm$  shows smaller corrections. For higher densities the limiting behavior is reached at larger fields (see the curve corresponding to  $E = 250V/cm$ ), though the interacting correction remains significative even for fields as low as  $E = 25V/cm$ .

Similar results, i.e. order of magnitude variations depending on the carrier density and quantitative importance of Coulomb interactions are obtained for the upstream penetration length  $L_u$  (see lower panel inset) too, with the key difference that in the “semiconductor de-

generate regime”  $L_u$  is strongly *reduced* by the electric field effect, being the product  $L_u \cdot L_d = L_s$  constant.

It is interesting to ask what happens in the high field regime  $e|E|L_s \gg (\epsilon_F, K_B T)$  when both temperature and carrier density varies. In Fig. 4, upper panel, we plot the high field limit of  $L_d$  in respect to carrier density and for three different temperatures,  $T = 1.6K$ ,  $T = 20K$  and  $T = 300K$ . In addition to the crossovers discussed in relation to Fig. 2, for low densities and  $T = 300K$  the system enters the non-degenerate regime  $\epsilon_F \ll K_B T$  (as shown in Fig. 1). In such region in fact the non-degenerate approximation coincides with the interacting calculation. Fig. 4 shows that the greatest variations due to the presence of the electric field are actually reached by lowering the temperature and correspond to the “degenerate semiconductor” regime.

The lower panel of Fig. 4 shows the importance of Coulomb corrections for the same parameters as the upper panel: again the largest corrections are present at  $T = 1.6K$  and low densities and are due to the Coulomb corrections to the spin stiffness. Even at temperatures as high as room temperature though, Coulomb interactions remain relevant and the correction can be as high as 30%. We underline that in this last case, such corrections are mainly given by the spin-drag effect<sup>5,7</sup> which enters the diffusion constant through the spin transresistivity.

### III. THE SPIN CURRENT

We will now focus on the spin-current for a non-magnetic system. Starting from the drift-diffusion Eq. (1), and imposing the conditions  $D_s = D_{\uparrow\uparrow} - D_{\uparrow\downarrow} = D_{\downarrow\downarrow} - D_{\downarrow\uparrow}$  and  $\mu_s = \mu_{\uparrow\uparrow} + \mu_{\uparrow\downarrow} = \mu_{\downarrow\downarrow} + \mu_{\downarrow\uparrow}$  which are obtained from the general formula for  $D_s$  and  $\mu_s$ <sup>5</sup> in the non-magnetic limit and in the regime linear in  $\nabla n_\alpha$ , the charge current becomes

$$\vec{j}(\vec{r}) := j_\uparrow(\vec{r}) + j_\downarrow(\vec{r}) = e\vec{E}\mu_s(n_\uparrow + n_\downarrow) \quad (9)$$

while the spin current assumes the form:

$$\begin{aligned} \vec{j}_s(\vec{r}) &:= j_\uparrow(\vec{r}) - j_\downarrow(\vec{r}) \\ &= e\vec{E}\mu_s(n_\uparrow - n_\downarrow) + eD_s\nabla(n_\uparrow - n_\downarrow) \quad (10) \\ &= \vec{j}P(x) + eD_s n \nabla P(x) \quad (11) \end{aligned}$$

with  $P(x) = (n_\uparrow - n_\downarrow)/n$  the density polarization. If we consider a spin unbalance injected at  $x = 0$ , i.e. such that in Eq. (7) either  $A = 0$  ( $x > 0$ ) or  $B = 0$  ( $x < 0$ ),  $\Delta n_\uparrow(\vec{r}, t) - \Delta n_\downarrow(\vec{r}, t)$  will have a simple exponential form; the upstream ( $x < 0$ ) (downstream ( $x > 0$ )) spin current will then be given by

$$\vec{j}_s^{u,d}(\vec{r}) = \left( \vec{j} \mp (-e)n \frac{D_s}{L_{u,d}} \hat{x} \right) P(x) \quad (12)$$

$$= (\vec{j} + \vec{j}_D^{u,d})P(x). \quad (13)$$

Eq. (13) is very interesting because it clearly shows how the spin current is composed:  $\vec{j}_s^{u,d}$  results in fact as the

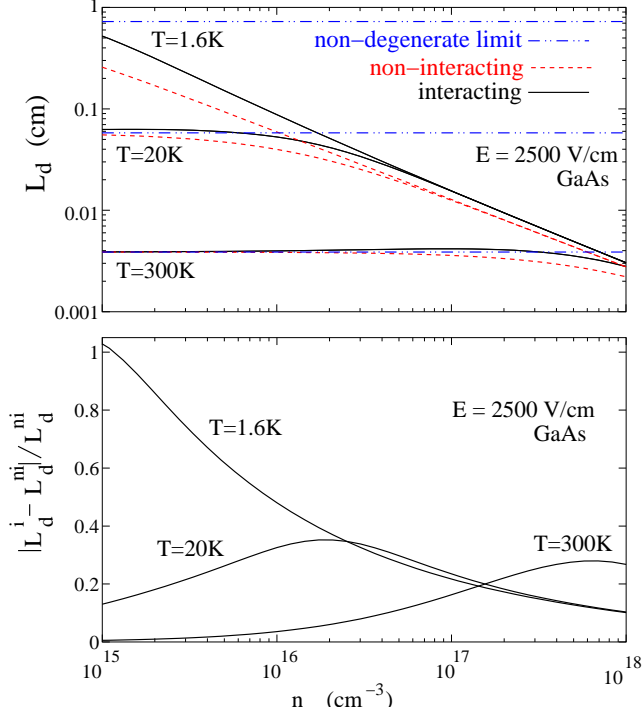


FIG. 4: Upper panel: downstream diffusion length  $L_d$  vs carrier density for GaAs parameters,  $T=1.6K$ ,  $20K$  and  $300K$  (as labelled) and  $E=2500V/cm$ . Solid line refers to the full interacting calculation, dashed line to the non-interacting approximation and dashed-double dotted line to the non-degenerate limit. Lower panel: correction to the non-interacting approximation  $|L_d^i - L_d^{ni}|/L_d^{ni}$  vs carrier density for GaAs parameters,  $T=1.6K$ ,  $20K$  and  $300K$  (as labelled) and  $E=2500V/cm$ .

sum of two distinct parts, the first corresponding to the *total* drift current  $\vec{j}$  and the second being a *total* diffusion current  $\vec{j}_D$ . Both the components are “weighted” by  $P(x)$ , the percentage of spin-polarized carriers. It is interesting to notice that in the downstream case,  $\vec{j} \parallel \vec{j}_D$ , so that both diffusion and drift phenomena positively contribute to the spin-current, while in the upstream case  $\vec{j}$  and  $\vec{j}_D$  are in competition. It is easy to see that in the limit of very large electric fields,  $1/L_d \rightarrow 0$  so that  $\vec{j}_s^d(\vec{r}) = \vec{j}P(x)$ , while  $1/L_u \rightarrow |E|\mu_s/D_s$  and  $\vec{j}_s^u(\vec{r})$  exactly vanishes. Keeping in mind that the diffusion constant increases by orders of magnitude when going from the non-degenerate to the degenerate regime, Eq. (12) suggests that to increment the spin current for a given electric field it is advised to go toward a degenerate regime (for example by lowering the temperature), increasing in this way the diffusive part of the current (while the drift term  $\vec{j}$  will remain constant). If instead the doping (or the temperature) is kept constant, an increase in the electric field will increase the drift current  $\vec{j}$ . In this last case though,  $1/L_d$  will decrease, and to the incremented  $\vec{j}$  will correspond a decreasing of  $\vec{j}_D^d$ . We

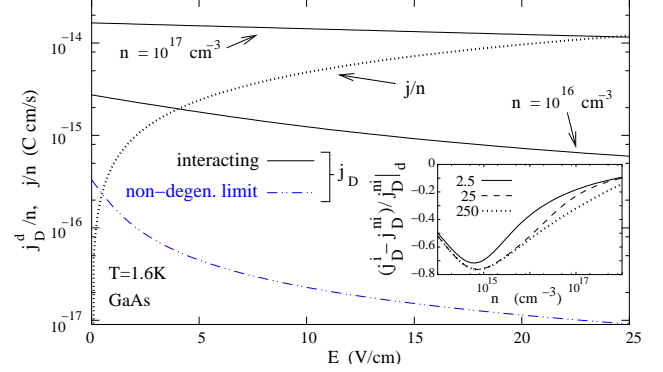


FIG. 5: Diffusion current density  $j_D$  and total current density  $j$  (rescaled by total carrier density  $n$ ) vs electric field  $E$  in the downstream direction for GaAs parameters,  $T=1.6K$  and two different carrier densities (as labelled). Solid lines refers to the interacting  $j_D/n$ , and the dashed-double-dot line to the non-degenerate limit of  $j_D/n$ . Dotted line refers to  $j/n$ . Inset: correction to the non-interacting approximation  $(j_D^i - j_D^{ni})/j_D^{ni}$  vs carrier density for  $E = 2.5$ ,  $25$ ,  $250V/cm$ .

are illustrating this behavior in Fig. 5. In such figure we plot  $j_D^d$  and  $j$  rescaled by the trivial (and common) dependence on the carrier density  $n$  in respect to the applied electric field and two different densities (as indicated) at  $T = 1.6K$ .  $j/n$  (dotted curve) does not depend over the density nor over Coulomb interaction. The fully interacting  $j_D^d/n$  corresponds to the solid line, and its non-degenerate limit to the dashed double-dotted line. If we fix the density and increase the electric field,  $j_D$  decreases and  $j$  increases; but if we fix the electric field (considering a moderate electric field), and increase the density,  $j_D$  increases while  $j$  does not change, so that there is no competition between the two quantities. We underline once more that this is not due to a trivial linear scaling with the carrier density, but to the behavior of the diffusion constant when entering the degenerate regime. Regarding the second factor of Eq. (13),  $P(x)$ , if we consider as injector a not-fully polarized metal, we deduce from the expression for  $P(0)$  (see next section), that, in the degenerate regime and for moderate fields,  $P(x)$  slightly increases with carrier density. This implies that our conclusions hold for the full spin current  $j_s^d$ .

The inset of Fig. 5 shows the Coulomb correction to  $j_D^d$  in respect to carrier density and for three different electric fields (as labelled in units of  $V/cm$ ). Again we see that, depending on the carrier density, they can be quite substantial.

#### IV. FM/NMS JUNCTION

We will now derive the relevant equations for a FM/NMS heterostructure. The schematic view of the system is illustrated in Fig. 6a. We will first derive ex-

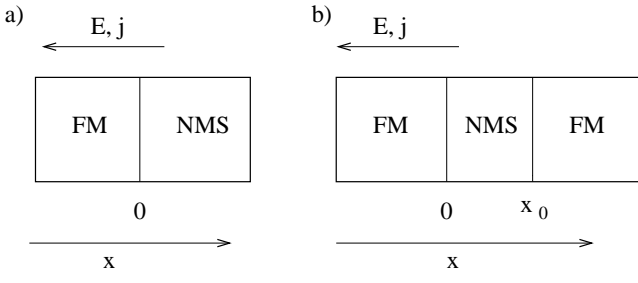


FIG. 6: Schematic view of the FM/NMS (left) and FM/NMS/FM (right) heterostructures considered in the paper.

plict expressions for the quantities of interest (density and current polarization, magnetoresistance, etc) in the general, interacting case, and then concentrate on the intermediate to degenerate regime. As underlined before, such regime is experimentally relevant, and in it Coulomb interactions are quantitative important.

Let us consider the Taylor expansion of the interacting chemical potential

$$\mu_{\sigma}^{chem}(n_{\uparrow}, n_{\downarrow}) = \mu_{0\sigma}^{chem} + \frac{\partial \mu_{\sigma}^{chem}}{\partial n_{\sigma}} \Delta n_{\sigma} + \frac{\partial \mu_{\sigma}^{chem}}{\partial n_{\bar{\sigma}}} \Delta n_{\bar{\sigma}} + \dots \quad (14)$$

If we use the relation

$$S_{\sigma\delta} \equiv \frac{\partial \mu_{\sigma}^{chem}}{\partial n_{\delta}} \quad (15)$$

between the  $\{\sigma\delta\}$  element of the spin-stiffness tensor and the chemical potential, and the local charge neutrality constraint Eq. (3), we can rewrite such potential as<sup>14</sup>

$$\mu_{\sigma}^{chem} \approx \mu_{0\sigma}^{chem} + (S_{\sigma\sigma} - S_{\sigma\bar{\sigma}}) \Delta n_{\sigma}. \quad (16)$$

The associated excess electrochemical potential then becomes

$$\Delta\mu_{\sigma} \equiv \mu_{\sigma} - \mu_{0\sigma}^{chem} \quad (17)$$

$$\approx (S_{\sigma\sigma} - S_{\sigma\bar{\sigma}}) \Delta n_{\sigma} + e\vec{E} \cdot \vec{x} + B. \quad (18)$$

Eq. (18) is general and valid both for polarized and non-magnetic materials.

By using the relation between the spin stiffness and the spin stiffness tensor components

$$S = (S_{\uparrow\uparrow} - S_{\uparrow\downarrow} + S_{\downarrow\uparrow} - S_{\downarrow\downarrow})/4, \quad (19)$$

the symmetries in the NMS material ( $S_{\uparrow\uparrow} - S_{\uparrow\downarrow} = S_{\downarrow\uparrow} - S_{\downarrow\downarrow}$ ), and the charge neutrality constraint, the electrochemical potential in the NMS ( $x > 0$ ) is given by

$$\begin{aligned} \Delta\mu_{\uparrow(\downarrow)} &= \pm SnP(x) + e\vec{E} \cdot \vec{x} + B \\ \Delta\mu_{\uparrow(\downarrow)} &= \pm \frac{D_s e}{\mu_s} (1 - \rho_{\uparrow\downarrow}/\rho_D) P(x) + e\vec{E} \cdot \vec{x} + B \end{aligned} \quad (20)$$

where we have used Eq. (6) in the second expression and the plus (minus) sign refers to the  $\uparrow$  ( $\downarrow$ ) spin component.

If we assume that the FM material (diluted magnetic semiconductor or metal) is in the “metallic” degenerate regime (as it is often the case), the electrochemical potential on the FM side ( $x < 0$ ) will be<sup>2,15</sup>

$$\begin{pmatrix} \Delta\mu_{\uparrow} \\ \Delta\mu_{\downarrow} \end{pmatrix} = e \frac{\vec{j} \cdot \vec{x}}{\sigma^f} \begin{pmatrix} 1 \\ 1 \end{pmatrix} + Ce \vec{j} \cdot \hat{x} \begin{pmatrix} 1/\sigma_{\uparrow}^f \\ -1/\sigma_{\downarrow}^f \end{pmatrix} \exp\left(\frac{x}{L_f}\right) \quad (21)$$

In this expression Coulomb interactions are included through  $\sigma_{\sigma}^f \equiv \sigma_{\sigma\sigma}^f + \sigma_{\sigma\bar{\sigma}}^f$ <sup>15</sup>. Since in such regime the spin transresistivity is much smaller than the Drude resistivity<sup>7</sup>, we will neglect the former in our calculations.

If we assume transparent interfaces, the boundary conditions to be satisfied at  $x = 0$  will be

$$j_s|_{0-} = j_s|_{0+} \quad (22)$$

$$\Delta\mu_{\uparrow}|_{0-} = \Delta\mu_{\uparrow}|_{0+} \quad (23)$$

$$\Delta\mu_{\downarrow}|_{0-} = \Delta\mu_{\downarrow}|_{0+}. \quad (24)$$

The spin current components are given by

$$e\vec{j}_{\sigma} = \sum_{\delta} \sigma_{\sigma\delta} \frac{\partial \Delta\mu_{\delta}}{\partial x} \hat{x}, \quad (25)$$

and the spin currents in the two materials will then become

$$\vec{j}_s^f = \vec{j} \left( p_f + \frac{2C}{L_f} \exp\left(\frac{x}{L_f}\right) \right) \quad (26)$$

$$\vec{j}_s^{sc} = P(x)(\vec{j} + \vec{j}_D^d) \quad (27)$$

where the indexes  $f$ ,  $sc$  correspond respectively to the FM and to the NMS,  $p_f \equiv (\sigma_{\uparrow}^f - \sigma_{\downarrow}^f)/(\sigma_{\uparrow}^f + \sigma_{\downarrow}^f)$  and  $\vec{j}_D^d$  is defined in Eq. (12).

By using Eqs. (20)-(27), after some straightforward algebra, we derive the expressions for the quantities of interest.

The electrochemical potential in the NMS semiconductor will be

$$\Delta\mu_{\uparrow(\downarrow)} = -SnP(0)[p_f \mp \exp(-x/L_d)] + e\vec{E} \cdot \vec{x}, \quad (28)$$

where the - (+) sign refers to the  $\uparrow$  ( $\downarrow$ ) spin component. In particular the expression for the interface band splitting is given by

$$\Delta\mu_{\uparrow}(0) - \Delta\mu_{\downarrow}(0) = 2SnP(0) \xrightarrow{E \rightarrow \infty} 2Sn p_f \quad (29)$$

We see that such splitting saturates for high electric fields. The relation  $Sn = \frac{D_s e}{\mu_s} (1 - \rho_{\uparrow\downarrow}/\rho_D)$  implies on the other hand that such limit can be increased by increasing the diffusion density  $D_s$  (for example by increasing the system density as previously discussed) or by exploiting the Coulomb drag effect.

The magnetoresistance (which is related to the electrochemical potential sum at the interface and will be discussed in details later) can be written as

$$R_m = -\frac{\Delta\mu_{\uparrow}(0) + \Delta\mu_{\downarrow}(0)}{2e|j|} = \frac{SnP(0)p_f}{e|j|}; \quad (30)$$

the equation for the injected density polarization is

$$P(0) = L_u \left( \frac{1}{L_u} - \frac{1}{L_d} \right) \frac{p_f}{\frac{\sigma_f}{\sigma_{sc}} \frac{(1-p_f^2)}{L_f} L_u (1 - \rho_{\uparrow\downarrow}/\rho_D) + 1} \quad (31)$$

while the one for the injected current polarization is

$$\alpha(0) = \frac{p_f}{\frac{\sigma_f}{\sigma_{sc}} \frac{(1-p_f^2)}{L_f} L_u (1 - \rho_{\uparrow\downarrow}/\rho_D) + 1}, \quad (32)$$

where we have use the relations  $E\mu_s/D_s = (1/L_u - 1/L_d)$ . We stress that Eqs. (28)-(32) are valid in all density and field regimes and represent the fully interacting expressions. It is interesting to notice that, the spin Coulomb drag enters such equations both implicitly through  $L_{u,d}$  and explicitly through the factor  $(1 - \rho_{\uparrow\downarrow}/\rho_D)$ . The latter should be expected by looking at Eq. (20), which implies that all quantities related to interface properties will contain explicitly such factor.  $\rho_{\uparrow\downarrow}$  is a negative quantity, so the presence of  $(1 - \rho_{\uparrow\downarrow}/\rho_D)$  in Eq. (30) will increase the magnetoresistance, while it will oppose spin injection in Eqs. (31) and (32). This is to be expected when thinking of the very nature of the SCD effect: in fact it tends to relax spin current *opposing relative motion* between up and down spin components.

Fig. 7 illustrates the behavior of the  $\uparrow$  and  $\downarrow$  electrochemical potentials (excluding the trivial linear dependence on  $x$ , as we will do for all the figure related to such quantities) across the FM/NMS junction ( $x = 0$ ) and for increasing field. In Fig. 7 the polarization in the FM is  $p_f = 0.5$ . The other parameters used in the calculations we present are  $n = 5 \cdot 10^{16} \text{ cm}^{-3}$ ,  $\sigma^f/\sigma_{sc} = 100$ ,  $L_f = 20 \text{ nm}$ ,  $L_s = 2 \mu\text{m}$ <sup>11</sup>. As the figure shows, the splitting of the FM sub-bands at the interface increases asymmetrically with the electric field depending on the ratio  $\sigma_{\uparrow}^f/\sigma_{\downarrow}^f$ . In the inset we plot the same electrochemical potentials but on the NMS side of the junction ( $x > 0$ ). As expected the potentials are now symmetric in respect to their asymptotic value and the extension of the polarized region in which  $\nabla\mu_{\sigma} \neq \text{const}$  extends in space as the electric field increases. As can be seen, the potential drop at the interface (the difference between the values of the electrochemical potentials at  $\pm\infty$ ), which is related to the magnetoresistance, increases with the field.

In the inset of Fig. 7, for  $E = 1000 \text{ V/cm}$ , we plot also the non-interacting approximation to the potentials (dashed line): as early discussed, at high fields, interactions increases in a noticeable way the spin penetration length  $L_d$  correspondingly increasing the extension of the polarized region.

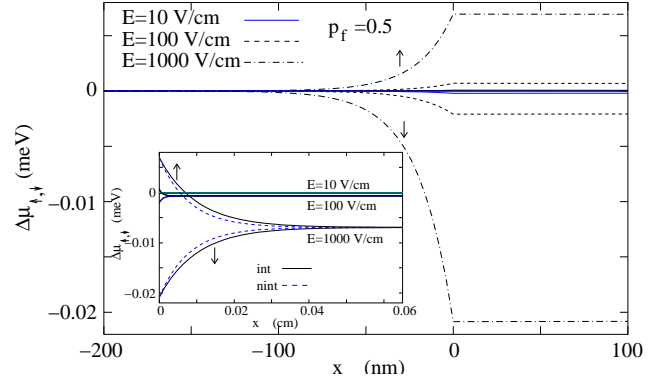


FIG. 7: Up and down electrochemical potentials (without the term linear in  $x$ ) at the junction vs  $x$  for three different fields (as labelled) and  $p_f = 0.5$ . Inset: as in main panel but on the NMS side of the junction. The non-interacting approximation (dashed line) is plotted as well.

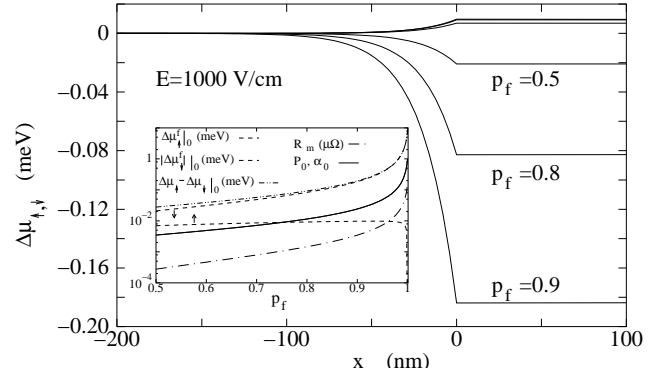


FIG. 8: Up and down electrochemical potentials at the junction (without the term linear in  $x$ ) vs  $x$  for three different FM polarizations (as labelled) and  $E = 1000 \text{ V/cm}$ . Inset: Up and down electrochemical potentials, their difference, the current and density polarizations calculated at  $x = 0$  as well as magnetoresistance  $R_m$  vs FM polarizations  $p_f$  for  $E = 1000 \text{ V/cm}$

Fig. 8 illustrates the influence of increasing the FM polarization on the electrochemical potentials at the junction and in the high field regime ( $E = 1000 \text{ V/cm}$ ). The inset shows in details the behavior of the related quantities as  $p_f$  is increased from 0.5 to full polarization. While most of the considered quantities (from the injected current and density polarizations to the sub-band splitting to the magnetoresistance) monotonically increase with the FM polarization to saturate when  $p_f = 1$ , the  $\uparrow$  sub-band split (dashed line labelled with  $\uparrow$ ) increases at first to rapidly drop to zero when the FM polarization saturates.

Fig. 9 shows the dependence of injected density and current polarizations at the interface for increasing electric field. As the field increases  $P_0$  saturates towards the

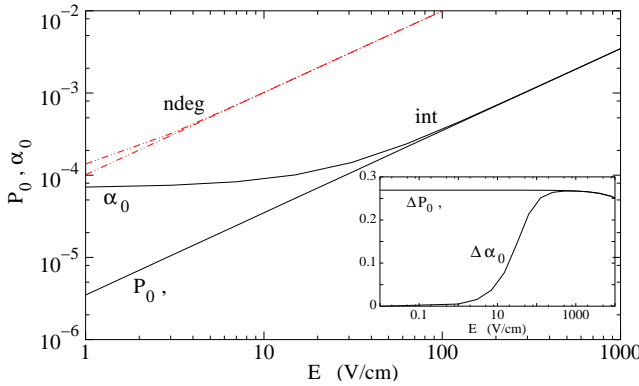


FIG. 9: Density and spin current polarizations  $P_0$  and  $\alpha_0$  (solid lines) vs electric field for  $p_f = 0.5$ . Their non-degenerate approximation (dashed-double-dot line) is plotted as well. Inset: correction to the non-interacting approximations  $\Delta P_0 \equiv (P_0^i - P_0^{ni})/P_0^{ni}$  and  $\Delta \alpha_0 \equiv (\alpha_0^i - \alpha_0^{ni})/\alpha_0^{ni}$  vs electric field.

$\alpha_0$  value. It is interesting also to compare the interacting calculation (solid line) with its non-degenerate approximation, calculated by inserting in Eqs. (31), (32) the non-degenerate approximations for  $L_{u,d}$  and setting  $\rho_{\uparrow\downarrow} = 0$ . As can be seen, such approximation overestimates the quantities by order of magnitudes, underestimating at the same time their difference at low electric fields.

In the inset we analyze the influence of Coulomb interactions on  $\alpha(0)$  and  $P(0)$  for increasing electric field. As can be expected by the lower panel of Fig. 3, for the density we are considering ( $n = 5 \times 10^{16} \text{ cm}^{-3}$ ) such influence is not negligible and of the order of 25%. For  $E \rightarrow 0$ , the ratio  $(P_0^i - P_0^{ni})/P_0^{ni} \rightarrow (D_s^i - D_s^{ni})/D_s^{ni}$ . Instead, as the field is increased inside the high field regime,  $L_u$  decreases and the Coulomb related term in Eqs. (31) and (32) becomes less important, so that the Coulomb correction starts to decrease.

### A. Magnetoresistance

A very important quantity for building “on-off” type devices as magnetic field sensors or read heads for magnetic hard disk drives<sup>16</sup> is the so called magnetoresistance  $R_m$ . It can be defined as the part of the equivalent resistance  $R_{eq}$  of the device which depends on its magnetic properties.

For the considered structure  $R_{eq}$  is given by

$$R_{eq} \equiv -\frac{\Delta\mu(\lambda_{sc}) - \Delta\mu(-\lambda_f)}{e|j|}, \quad (33)$$

where  $\lambda_{sc(f)}$  are the device lengths in the NMS and FM regions ( $\lambda_{sc} \approx nL_s$  and  $\lambda_f \approx nL_f$ ),  $\Delta\mu = (\Delta\mu_{\uparrow} + \Delta\mu_{\downarrow})/2$  and  $\Delta\mu$  indicates the increment (decrement) in the electrochemical potential in respect to the situation in which

no electric field is applied, and no junction is present. We will define  $R_m$  as the nontrivial part of  $R_{eq}$  when  $n \gg 1$ . For a FM/NMS junction we obtain

$$R_m = \frac{L_s}{\sigma_{sc} \mu_s |E| \tau_s} (1 - \frac{\rho_{\uparrow\downarrow}}{\rho_D}) p_f P(0). \quad (34)$$

Eq. (34) is very interesting: it clearly shows that  $R_m$  depends on the intrinsic resistance of the NMS material  $L_s/\sigma_{sc}$ , on the ratio between diffusion and drift lengths  $L_s/\mu_s |E| \tau_s$  and it manifest the dependence of  $R_m$  on the drag effect. It also shows that the magnetoresistance is proportional to the probability  $p_f P(0)$  that a spin crosses the interface without loosing its spin polarization, i.e. it preserves its magnetic properties when entering the NMS.

In Fig. 10 we plot the magnetoresistance  $R_m$  in respect to the electric field for  $p_f = 0.5$  (upper panel) and  $p_f = 1$  (lower panel). As already discussed, we see that while the increased FM polarization increases the value of  $R_m$  (see inset of Fig. 8, dashed-dot line), the electric field, increasing the spin penetration inside the NMS, and reducing the change in magnetic properties across the device, destroys the magnetoresistance. Again we plot for comparison the non-degenerate approximation to  $R_m$  (dashed-double-dot line): we see that, such approximation can heavily underestimate  $R_m$  even at low and intermediate electric fields.

The inset presents the Coulomb interaction effects in respect to the non-interacting approximation of  $R_m$  for increasing electric field and polarization. We see that Coulomb interaction effects become important as both field and  $p_f$  increases.

## V. FM/NMS/FM STRUCTURE

We will now consider the tri-layer structure of Fig. 6b. According to Eq. (7) and to the local charge neutrality constraint, in the NMS the excess spin density components are given by

$$\Delta n_{\uparrow(\downarrow)} = \pm \left[ A_0 \exp(-\frac{x}{L_d}) + A_1 \exp(\frac{(x - x_0)}{L_u}) \right] \quad (35)$$

where  $x_0 > 0$  corresponds to the second interface and the minus sign to the  $\downarrow$  component. The chemical potentials in the three materials are now

$$\begin{aligned} \left( \frac{\Delta\mu_{\uparrow}}{\Delta\mu_{\downarrow}} \right)_L &= e \frac{\vec{j} \cdot \vec{x}}{\sigma_L^f} \begin{pmatrix} 1 \\ 1 \end{pmatrix} \\ &+ C_L e \vec{j} \cdot \hat{x} \begin{pmatrix} 1/\sigma_{\uparrow,L}^f \\ -1/\sigma_{\downarrow,L}^f \end{pmatrix} \exp(\frac{x}{L_L^f}) \end{aligned} \quad (36)$$

$$\Delta\mu_{\uparrow(\downarrow)} = \pm \frac{D_s e}{\mu_s} (1 - \rho_{\uparrow\downarrow}/\rho_D) P(x) + e \vec{E} \cdot \vec{x} + B_{37} \quad (37)$$

$$\left( \frac{\Delta\mu_{\uparrow}}{\Delta\mu_{\downarrow}} \right)_R = e \vec{j} \cdot \hat{x} \left( \frac{x}{\sigma_R^f} + B_f \right) \begin{pmatrix} 1 \\ 1 \end{pmatrix} \quad (38)$$

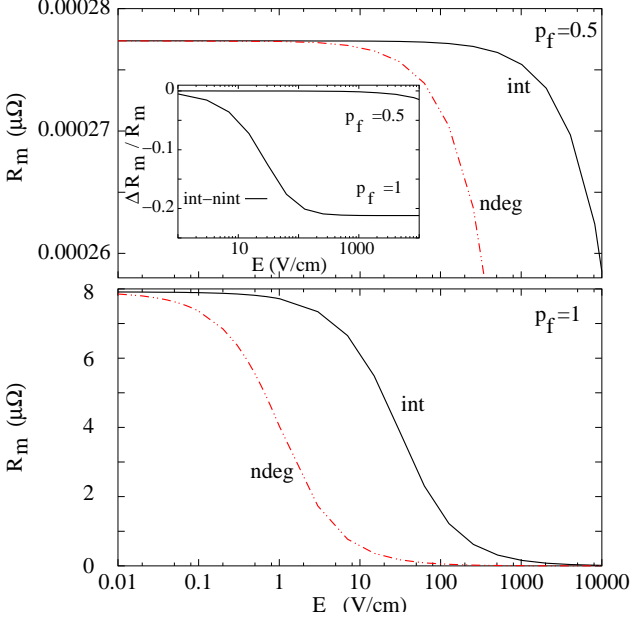


FIG. 10: Upper panel: magnetoresistance  $R_m$  vs electric field for  $p_f = 0.5$ . Its non-degenerate approximation is plotted as well (dashed-double-dot line). Inset: Correction to the non-interacting approximation  $\Delta R_m / R_m \equiv (R_m^i - R_m^{ni}) / R_m^{ni}$  vs electric field for  $p_f = 0.5$  and  $p_f = 1$  (as labelled). Lower panel: as for the upper panel but for  $p_f = 1$

$$+ C_R e \vec{j} \cdot \hat{x} \begin{pmatrix} 1/\sigma_{\uparrow,R}^f \\ -1/\sigma_{\downarrow,R}^f \end{pmatrix} \exp\left(-\frac{(x-x_0)}{L_R^f}\right) \quad (38)$$

where the indices  $L$ ,  $R$  stay for left and right ferromagnets and the  $+$  ( $-$ ) sign in Eq. (37) corresponds to the  $\uparrow$  ( $\downarrow$ ) component. The six constants  $\{A_0, A_1, B_{sc}, B_f, C_L, C_R\}$  will be determined by boundary conditions similar to the ones for the single interface, i.e.

$$j_s|_{0^-, x_0^-} = j_s|_{0^+, x_0^+} \quad (39)$$

$$\Delta\mu_{\uparrow}|_{0^-, x_0^-} = \Delta\mu_{\uparrow}|_{0^+, x_0^+} \quad (40)$$

$$\Delta\mu_{\downarrow}|_{0^-, x_0^-} = \Delta\mu_{\downarrow}|_{0^+, x_0^+}. \quad (41)$$

First of all let us consider the spin density and current polarizations. In order to write the expressions for these quantities we need to derive the expressions for  $A_0$ ,  $A_1$ . For general polarizations  $p_L^f$ ,  $p_R^f$ , after some algebra, the expressions for  $A_0$ ,  $A_1$  can be written as

$$A_0 = \frac{n}{2} L_u \left( \frac{1}{L_u} - \frac{1}{L_d} \right) \left( p_f^L - \exp\left(-\frac{x_0}{L_u}\right) \frac{d_L^-}{d_R^+} p_f^R \right) \cdot \left[ u_L^+ - \exp\left(-x_0 \left( \frac{1}{L_u} + \frac{1}{L_d} \right)\right) u_R^- \frac{d_L^-}{d_R^+} \right]^{-1} \quad (42)$$

$$A_1 = -\frac{n}{2} L_d \left( \frac{1}{L_u} - \frac{1}{L_d} \right) \left( p_f^R - \exp\left(-\frac{x_0}{L_d}\right) \frac{u_R^-}{u_L^+} p_f^L \right)$$

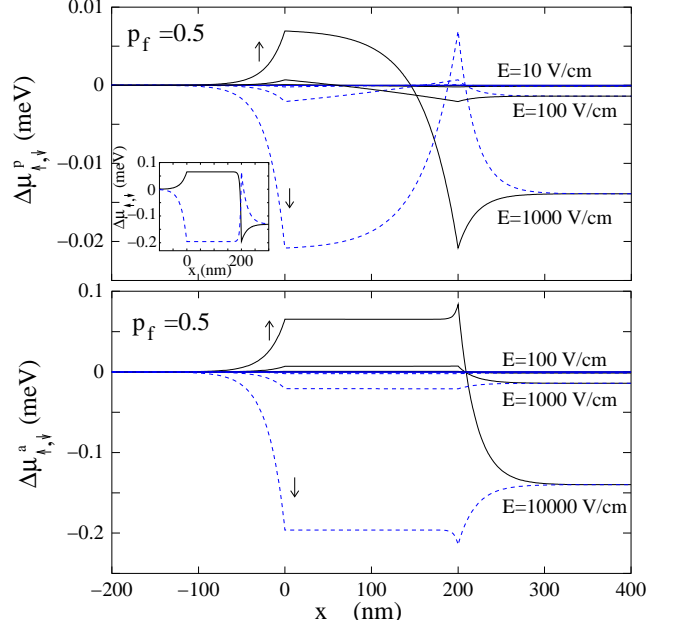


FIG. 11: Upper panel: Up (solid line) and down (dashed line) electrochemical potentials (without the term linear in  $x$ ) vs  $x$  for three different fields (as labelled) and  $p_f = 0.5$ . The two ferromagnet polarizations are *parallel*. Inset: as in main panel but for  $E=10000$  V/cm. Lower panel: Up (solid line) and down (dashed line) electrochemical potentials (without the term linear in  $x$ ) vs  $x$  for three different fields (as labelled) and  $p_f = 0.5$ . The two ferromagnet polarizations are *antiparallel*.

$$\cdot \left[ d_R^+ - \exp\left(-x_0 \left( \frac{1}{L_u} + \frac{1}{L_d} \right)\right) d_L^- \frac{u_R^-}{u_L^+} \right]^{-1}, \quad (43)$$

where

$$d_{R,L}^{\pm} \equiv 1 \pm G_{R,L} \frac{L_d}{L_{R,L}^f} \quad (44)$$

$$u_{R,L}^{\pm} \equiv 1 \pm G_{R,L} \frac{L_u}{L_{R,L}^f}, \quad (45)$$

and

$$G_{R,L} \equiv \frac{\sigma_{R,L}^f}{\sigma_{sc}^f} [1 - (p_{R,L}^f)^2] \left( 1 - \frac{\rho_{\uparrow\downarrow}}{\rho_D} \right). \quad (46)$$

The spin density and current polarizations are then expressed as

$$P(x) = \frac{2}{n} \left[ A_0 \exp\left(-\frac{x}{L_d}\right) + A_1 \exp\left(\frac{(x-x_0)}{L_u}\right) \right] \quad (47)$$

$$\alpha(x) = \frac{2}{n} \left( \frac{1}{L_u} - \frac{1}{L_d} \right)^{-1} \cdot \left[ A_0 \exp\left(-\frac{x}{L_d}\right) \frac{1}{L_u} - A_1 \exp\left(\frac{(x-x_0)}{L_u}\right) \frac{1}{L_d} \right] \quad (48)$$

In the interesting case in which  $p_L^f = \pm p_R^f = p^f$  (parallel

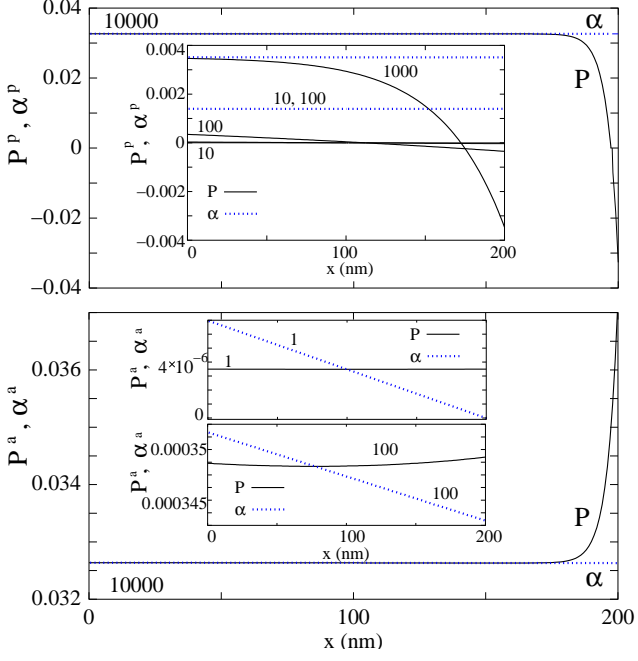


FIG. 12: Upper panel: density (solid line) and current (dot line) polarizations vs  $x$  for  $E=10000$  V/cm and  $p_f = 0.5$ . The two ferromagnet polarizations are *parallel*. Inset: density (solid line) and current (dot line) polarizations vs  $x$  for three different fields (as labelled in units of V/cm) and  $p_f = 0.5$ . The two ferromagnet polarizations are *parallel*. Lower panel: density (solid line) and current (dot line) polarizations vs  $x$  for  $E=10000$  V/cm and  $p_f = 0.5$ . The two ferromagnet polarizations are *antiparallel*. Upper inset: as in main panel but for  $E=1$  V/cm. Lower inset: as in main panel but for  $E=100$  V/cm.

and anti-parallel polarization of the two FM's considered, for the rest, equivalent) the current polarization at the two interfaces becomes:

$$\alpha(0) = \frac{p^f}{d_R^+ u_L^+ - \exp(-x_0 \left( \frac{1}{L_u} + \frac{1}{L_d} \right)) d_L^- u_R^-} \cdot \left[ d_R^+ - \exp(-x_0 \left( \frac{1}{L_u} + \frac{1}{L_d} \right)) u_R^- \right. \\ \left. \pm \exp(-\frac{x_0}{L_u}) \frac{G_L}{L_L^f} (L_u + L_d) \right] \quad (49)$$

$$\alpha(x_0) = \frac{\pm p^f}{d_R^+ u_L^+ - \exp(-x_0 \left( \frac{1}{L_u} + \frac{1}{L_d} \right)) d_L^- u_R^-} \cdot \left[ u_L^+ - \exp(-x_0 \left( \frac{1}{L_u} + \frac{1}{L_d} \right)) d_L^- \right. \\ \left. \pm \exp(-\frac{x_0}{L_d}) \frac{G_R}{L_R^f} (L_u + L_d) \right], \quad (50)$$

where the upper (lower) sign refers to the parallel (antiparallel) configuration.

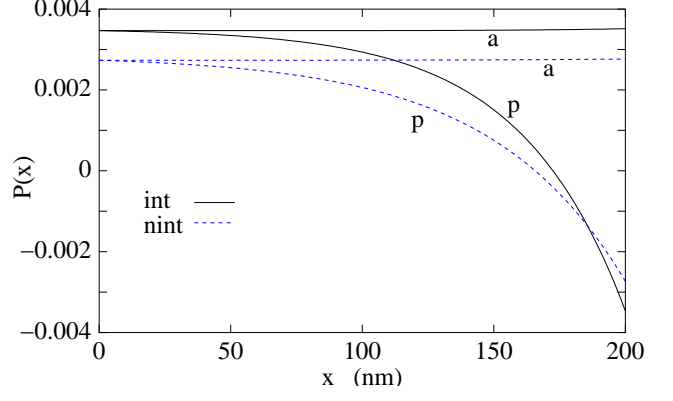


FIG. 13: Density polarization  $P(x)$  vs  $x$  for the parallel (labelled as “p”) and antiparallel (“a”) configurations (solid line). its non-interacting approximation (dashed line) is plotted as well.

The expressions for the other constants which appear in the electrochemical potentials are then given by

$$B_{sc} = -SnP(0)p_L^f \quad (51)$$

$$B_f = -\frac{x_0}{\sigma_R^f} + \frac{|E|}{|j|}x_0 + \frac{Sn}{e|j|}[p_L^f P(0) - p_R^f P(x_0)] \quad (52)$$

$$C_L = -\frac{Sn}{2} \frac{P(0)}{e|j|} \sigma_L^f (1 - p_L^{f2}) \quad (53)$$

$$C_R = -\frac{Sn}{2} \frac{P(x_0)}{e|j|} \sigma_R^f (1 - p_R^{f2}) \quad (54)$$

In Fig. 11 we plot the behavior of the  $\uparrow$  (solid lines) and  $\downarrow$  (dashed lines) electrochemical potentials in the tri-layer structure for the interesting case in which the NMS width  $x_0$  is much smaller than the diffusion length ( $x_0 = L_s/10$ ). The upper panel shows the electrochemical potentials when a parallel configuration ( $p_{fL} = p_{fR} = 0.5$ ) is considered. The lower panel shows the two junction system when the polarizations of the two FM's are opposite (anti-parallel case). For both configurations, as the field is increased the potential drop due to the presence of the NMS material increases.

We notice immediately that in the parallel case the two spin components of the electrochemical potentials cross. Such crossing was predicted to occur in Ref. 1 and is necessary in order to obtain a different potential drop for the  $\uparrow$  and  $\downarrow$  spin components and hence a finite current polarization even at low electric fields. A clear effect of the electric field enhancement is to “push” the crossing between  $\uparrow$  and  $\downarrow$  components toward the second interface by increasing the penetration length  $L_d$  relative to the first interface and decreasing the upstream penetration length  $L_u$  relative to the second interface. This behavior becomes extreme for very high fields (see inset where  $E = 10000$  V/cm), where after an almost constant behavior, the electrochemical potentials suddenly switch before the second interface.

In the antiparallel configuration (lower panel), while the potential drop across the whole structure behaves similarly to the parallel case, the electrochemical potentials do not cross (this behavior destroys the spin current at very low fields<sup>1</sup>). They present instead a quite distinct feature: for increasing fields a spin accumulation builds up just before the second interface, underlining the increasing resistance that spins encounter in crossing such interface when the field (and the polarization inside the NMS) increases. This anticipates that in this configuration the magnetoresistance is expected to increase with increasing applied electric field.

Fig. 12 presents the behavior of the density (solid lines) and current (dotted line) polarizations in respect to  $x$  for both the parallel (upper panel) and the anti-parallel (lower panel) configuration, when the field is increased from the low field regime ( $E = 1V/cm$ ,  $E = 10V/cm$ ), to the intermediate ( $E = 100V/cm$ ), to the high field one ( $E = 1000V/cm$ ,  $E = 10000V/cm$ ). The main panel presents the highest field situation. In both configurations, as expected from the behavior in the single junction system (see Fig. 9), for low to intermediate fields  $P(0) < \alpha(0)$ , while  $P(0) \rightarrow \alpha(0)$  in the high field regime. On the other side, in the parallel configuration, while, due to the choice  $x_0 \ll L_s$ ,  $\alpha(x)$  is basically constant even at very low fields, we see that when the two electrochemical potentials cross, the density polarization  $P(x)$  switches sign.

The situation is different in the antiparallel case in which, at low to intermediate fields, to an almost constant  $P(x)$  corresponds a constant drop of the current polarization  $\alpha(x)$  in respect to  $x$ . For very low fields ( $E = 1V/cm$ ), and just before the II junction, it becomes even slightly negative. This is due to the difficulty in establishing a spin current through the system due to the abrupt decrease of the  $\uparrow$ -spin density of states in the second ferromagnet. When the field is increased, the decrease of the current density becomes less drastic while a spin accumulation starts to build up at the second interface (see lower panel of the inset). In the high field regime finally, it is possible to establish a basically constant spin density current through the device, at the price of building up a strong spin density accumulation just before the second interface (main lower panel).

In Fig. 13 we present the influence of Coulomb interactions on the density spin polarization  $P(x)$  across the NMS in the parallel (labelled by “p”) and antiparallel (labelled by “a”) configuration for  $E = 1000V/cm$ . The non-interacting approximation corresponds to the dashed lines. Again, as for the one-junction case, the interaction correction is of the order of 20-25%.

### A. Magnetoresistance

Let us now concentrate on the magnetoresistance.  $R_{eq}$  in the FM/NMS/FM structure is given by

$$R_{eq} \equiv -\frac{\Delta\mu(x_0 + \lambda_{f,R}) - \Delta\mu(-\lambda_{f,L})}{e|j|}, \quad (55)$$

where NMS extends from 0 to  $x_0$ . By writing  $\lambda_{f,R(L)} = nL_{fR(L)}$  and using for the electrochemical potentials Eqs. (36),(37) and (38), we obtain

$$R_{eq} = n \left[ \frac{L_{fR}}{\sigma_{fR}} + \frac{L_{fL}}{\sigma_{fL}} \right] + \left[ \frac{x_0}{\sigma_{sc}} \right] + \frac{L_s}{\sigma_{sc}} (1 - \exp(-n)) \frac{L_s}{\mu_s |E| \tau_s} (1 - \frac{\rho_{\uparrow\downarrow}}{\rho_D}) \cdot [p_{fL}P(0) - p_{fR}P(x_0)] \quad (56)$$

The first line is clearly the trivial, non-magnetic term. For  $n \gg 1$ ,  $R_m$  will be given by

$$R_m = \frac{L_s}{\sigma_{sc}} \frac{L_s}{\mu_s |E| \tau_s} (1 - \frac{\rho_{\uparrow\downarrow}}{\rho_D}) \cdot [p_{fL}P(0) - p_{fR}P(x_0)] \quad (57)$$

The above equation shows that  $R_m$  (i) is proportional to the intrinsic resistance of the paramagnet  $\frac{L_s}{\sigma_{sc}}$ ; (ii) it depends directly on the ratio between the diffusion length  $L_s = \sqrt{D_s \tau_s}$  and the drift length  $\mu_s |E| \tau_s$ ,i.e. it tends to diminishes with increasing field since the spins will be drifted longer and less resistance occurs (iii) it depends directly on the spin drag which enhances it; (iv) it is proportional to the difference  $p_{fL}P(0) - p_{fR}P(x_0) = |p_{fL}P(0)| + |p_{fR}P(x_0)|$ . This term can be seen as the probability that magnetic properties remain relevant through the whole structure. It implies that, as long as the products  $|p_f P|$  are not vanishing, magnetoresistance is accumulated at the different junctions . (v)in the important case in which  $p_L^f = \pm p_R^f = p^f$ , the last factor becomes  $p_f[P(0) \mp P(x_0)]$ : this shows that in the antiparallel case the magnetoresistance is proportional to the sum of the density polarizations just after the first interface and before the second one. This implies that it is enhanced by the spin accumulation due to the increasing of the electric field (see Fig. 12).

Fig. 14 illustrates the behavior of the magnetoresistance  $R_m$  in respect to the electric field. The upper panel refers to the parallel configuration. We clearly see that the field decreases the magnetoresistance. The non-degenerate approximation (dashed double-dot line) is shown for comparison: as in the single junction system, it clearly overestimates the field effect. The inset shows the corresponding situation for the antiparallel case: as anticipated, in this case the magnetoresistance is increased by the applied electric field. Again the non-degenerate approximation overestimates the effect. The lower panel presents the ratio of the difference between the parallel  $R_m^p$  and the antiparallel  $R_m^a$  magnetoresistances to  $R_m^p$ . Such ratio is increased by the field effect.

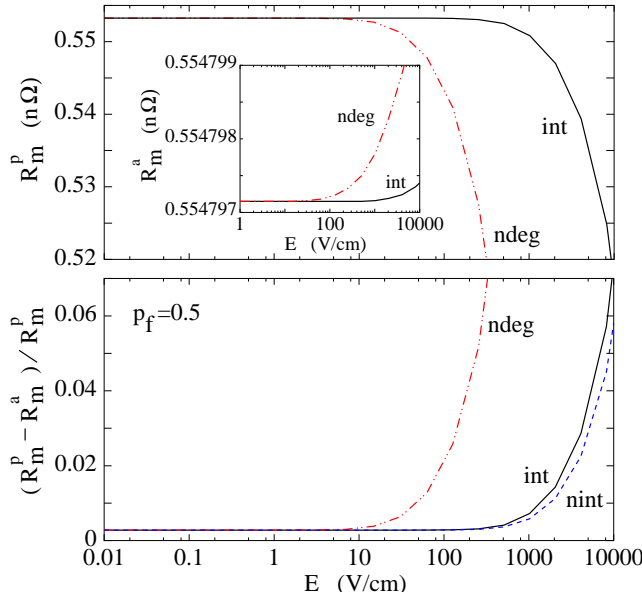


FIG. 14: Upper panel: magnetoresistance  $R_m$  for the parallel configuration vs electric field for  $p_f = 0.5$ . Its non-degenerate approximation (dashed-double-dot line) is plotted for comparison. Inset: as for main panel, but for the antiparallel configuration. Lower panel: magnetoresistance variation from the parallel to the antiparallel configuration vs electric field for  $p_f = 0.5$ . Its non-degenerate (dashed-double-dot line) and non-interacting approximations (dashed line) are plotted for comparison.

The non-degenerate and non-interacting approximations are shown for comparison. From Fig. 14 we see that Coulomb interactions at high fields and at the considered density can influence the result by 20-25%, while, even at low fields, the non-degenerate approximation behaves very poorly. It would be interesting to study the effect of different polarizations ( $p_{fL} \neq p_{fR}$ ) in the two FM's on the magnetoresistance in both the parallel and the anti-parallel configurations as well as the behavior of the system in the antiparallel configuration when the FM magnetization saturates or when field effects becomes important also inside the FM. This will be the subject of future analysis.

## VI. CONCLUSIONS

We have presented a detailed study of spin injection into degenerate semiconductors, analyzing the combined effects of applied electric field, carrier density and Coulomb interactions.

In particular we have focused on ferromagnet/non-magnetic semiconductor and ferromagnet/non-magnetic semiconductor/ferromagnet structures, carefully comparing the behavior of the relevant quantities (electrochemical potentials, spin density, magnetoresistance...)

when the polarization of the second ferromagnet is switched from parallel to antiparallel and its absolute value and the electric field are increased.

We have pointed out, in the anti-parallel case, that the presence of a spin-current through the device is related to the onset of a spin accumulation at the second interface, which is built-up by the increase of the spin-current drift term due to the strong applied electric field.

We have proposed a general formalism which includes Coulomb interactions and applies to such structures independently from their carrier density regime. In particular it allows also the study of heterostructures in the intermediate regime  $\varepsilon \approx k_B T$ . Exact expressions for the case in which a non-interacting degenerate system is considered have been also provided.

Our calculations show that, in the experimentally important regime  $\varepsilon_f \gtrsim k_B T$ , Coulomb corrections are relevant; they also demonstrate that non-degenerate approximations, when extended to the wrong regime, behave very poorly.

## APPENDIX A: LIMIT OF THE CHEMICAL POTENTIAL APPROXIMATION

The approximation we proposed for the chemical potential Eq. (16) can be thought at the first sight to be valid only in the low polarization limit  $P(x) \ll 1$ .

In this appendix we want to estimate the limits of such approximation in the important case of a degenerate system.

In a non-interacting system the Taylor expansion Eq. (14) becomes

$$\mu_{\sigma}^{chem} = \mu_{0\sigma}^{chem} + \frac{\partial \mu_{\sigma}^{chem}}{\partial n_{\sigma}} \Delta n_{\sigma} + \frac{1}{2} \frac{\partial^2 \mu_{\sigma}^{chem}}{\partial n_{\sigma}^2} \Delta n_{\sigma}^2 + \dots \quad (A1)$$

In a degenerate non-magnetic system, the chemical potential (up to terms of order  $T^2$ ) is given by

$$\mu_{\sigma}^{chem} = \varepsilon_{F\sigma} = \frac{\hbar^2}{2m} (6\pi^2 n_{\sigma})^{2/3} \quad (A2)$$

Truncating Eq. (A1) up to first order, is equivalent to request

$$\frac{1}{2} \left| \frac{\partial^2 \mu_{\sigma}^{chem}}{\partial n_{\sigma}^2} \Delta n_{\sigma}^2 \right| \ll \left| \frac{\partial \mu_{\sigma}^{chem}}{\partial n_{\sigma}} \Delta n_{\sigma} \right|, \quad (A3)$$

which, using Eq. (A2) becomes

$$P(x) \ll 6. \quad (A4)$$

The above equation implies that, in the important case of a degenerate system, our approximation is valid up to injected polarizations of at least  $P(x) \sim 0.5^{17}$ . In the special case of a single junction heterostructure it remains valid up to density polarizations of the order of 1. This is shown in Fig. 15, where the effects of the chemical potential approximation discussed at the beginning

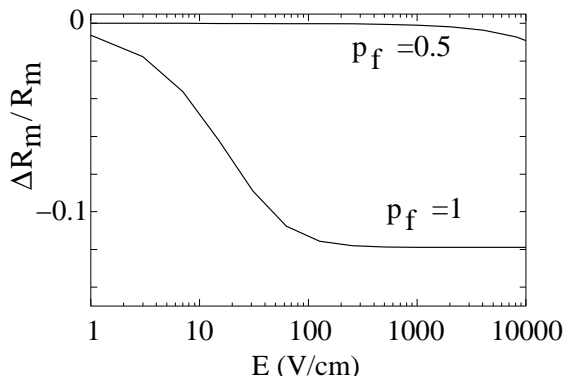


FIG. 15: Correction to the (non-interacting) degenerate approximation for  $R_m$ ,  $\Delta R_m/R_m \equiv (R_m^{exa} - R_m^{deg})/R_m^{deg}$  vs electric field for  $p_f = 0.5$  and  $p_f = 1$  (as labelled). Here  $R_m^{exa}$  corresponds to the (non-interacting) exact degenerate calculation.

of Sec.IV are presented for increasing electric field and FM polarization. Fig. 15 compares the results obtained for  $R_m$  in the FM/NMS structure using the (degenerate) approximation to the chemical potential, with the corresponding exact degenerate results (see Appendix B). The figure shows that our approximation for the chemical potential gives reasonably small errors (at most of the order of 10%) even for  $p_f = 1$ . We caution though that this feature cannot be blindly generalized.

Since  $|P(x)| \leq p_f$  and the equality corresponds to the

high field limit, we have analyzed systems in which  $p_f$  satisfies the same limitations found for  $P(x)$ .

## APPENDIX B: NON-INTERACTING DEGENERATE SYSTEM

If we consider a non-interacting, degenerate NMS, Eq. (17) for the excess electrochemical potential becomes

$$\Delta\mu_\sigma = e\vec{E} \cdot \vec{x} + (\varepsilon_{F\sigma} - \varepsilon_{F\sigma}^0) + B \quad (B1)$$

$$= e\vec{E} \cdot \vec{x} + \varepsilon_{F\sigma}^0 \left[ (1 \pm P(x))^{2/3} - 1 \right] + B \quad (B2)$$

where the  $+$ ( $-$ ) sign corresponds to  $\sigma = \uparrow$  ( $\downarrow$ ) and  $\varepsilon_{F\sigma}^0$  is the Fermi energy of the unperturbed system.

Applying the conditions (22)-(24), we can now derived the equations for the injected density polarization  $P(0)$

$$\begin{aligned} & - \frac{eL_f}{2\varepsilon_{F\sigma}^0} (|j| + |j_D|) \frac{4}{\sigma_f} \frac{1}{1 - p_f^2} P(0) - \{ [1 + P(0)]^{2/3} \\ & - [1 - P(0)]^{2/3} \} + \frac{e|j|L_f}{2\varepsilon_{F\sigma}^0} p_f \frac{4}{\sigma_f} \frac{1}{1 - p_f^2} = 0. \end{aligned} \quad (B3)$$

Once  $P(0)$  is known it is easy to derive all other quantities of interest.

A similar scheme can be applied to the two junction system, where we obtain a system of two implicit equations for the two quantities  $P(0)$  and  $P(x_0)$ , which must be solved self consistently .

---

<sup>1</sup> G. Schmidt, D. Ferrand, L. W. Molenkamp, A.T. Filip and B.J. van Wees, *Phys. Rev. B* **62**, R4790 (2000)  
<sup>2</sup> Z.G. Yu and M.E. Flatté, *Phys. Rev. B* **66**, 235302 (2002)  
<sup>3</sup> J.M. Kikkawa and D.D. Awschalom, *Nature* **397**, 139 (1999)  
<sup>4</sup> G. Schmidt, C. Gould, P. Grabs, A. M. Lunde, G. Richter, A. Slobodskyy, and L. W. Molenkamp, cond-mat/0206347  
<sup>5</sup> I. D'Amico and G. Vignale, *Phys. Rev. B* **65**, 085109 (2002)  
<sup>6</sup> Eqs. (5) and (6) correspond to the limit in which the Drude scattering times for  $\uparrow$  and  $\downarrow$  spin population are equal; for the more general expressions see Ref. 5.  
<sup>7</sup> I. D'Amico and G. Vignale, *Phys. Rev. B* **62**, 4853 (2000)  
<sup>8</sup> I. D'Amico and G. Vignale, *Europhys. Lett.* **55** (2001).  
<sup>9</sup> M.E. Flatté and J.M. Byers, *Phys. Rev. Lett.* **84**, 4220 (2000)  
<sup>10</sup> The term “diffusion” is in this case misleading, since for high electric fields  $L_{u,d}$  strongly dependent over the drift term. For this reason we prefer to refer to them as “penetration” lengths.  
<sup>11</sup> In bulk GaAs, taking as an estimate for low-T  $\tau_s$  the spin

decoherence values reported in Ref. 18, and for  $D_s$  our calculated value, we find that,  $L_s = \sqrt{\tau_s D_s} \approx 2\mu\text{m}$  over the range  $10^{16}\text{cm}^{-3} < n < 10^{18}\text{cm}^{-3}$ . In (Zn, Be)Se a spin diffusion length of at least  $L_s = 2\mu\text{m}$  is considered a reasonable value (L. W. Molenkamp and G. Schmidt, private communication).

<sup>12</sup> P.C. van Son, H. van Kempen, and P. Wyder, *Phys. Rev. Lett.* **58**, 2271 (1987)

<sup>13</sup> The interacting and non-interacting systems are defined as having the same diffusion length  $L_s$  when no external field is applied.

<sup>14</sup> see also Appendix A.

<sup>15</sup> G. Vignale and I. D'Amico, preprint

<sup>16</sup> G.A. Prinz, *Science* **282**, 1660 (1998)

<sup>17</sup> If we apply the same analysis to the non-degenerate case, where  $\mu_\sigma^{chem} \sim \ln n_\sigma$ , we obtain  $P(x) \ll 2$ .

<sup>18</sup> J.J. Kikkawa and D.D. Awschalom, *Phys. Rev. Lett.* **80**, 4313 (1998)